**AALBORG
UNIVERSITY**

Evaluation of a surrogate contact model in force-dependent kinematic simulations of total knee replacement

Marra, Marco A.; Andersen, Michael S.; Damsgaard, Michael; Koopman, Bart (H.F.J.M); Janssen, Dennis; Verdonschot, Nico

American Society of Mechanical Engineers

ASME Accepted Manuscript Repository

Evaluation of a Surrogate Contact Model in Force-Dependent Kinematic Simulations of Total Knee Replacement

Marco A. Marra[1]

Radboud University Medical Center, Radboud Institute for Health Sciences, Orthopaedic Research Laboratory

P.O.Box 9101, 6500 HB Nijmegen, The Netherlands

Marco.Marra@radboudumc.nl

Michael S. Andersen

Aalborg University, Department of Mechanical and Manufacturing Engineering

Fibigerstraede 16, DK-9220 Aalborg, Denmark

msa@m-tech.aau.dk

Michael Damsgaard

AnyBody Technology A/S

Niels Jernes Vej 10, DK-9220 Aalborg, Denmark

md@anybodytech.com

Bart F.J.M. Koopman

University of Twente, Department of Biomechanical Engineering

P.O.Box 217, 7500 AE Enschede, The Netherlands

h.f.j.m.koopman@utwente.nl

Dennis Janssen

Radboud University Medical Center, Radboud Institute for Health Sciences, Orthopaedic Research Laboratory

P.O.Box 9101, 6500 HB Nijmegen, The Netherlands

Dennis.Janssen@radboudumc.nl

Nico Verdonschot

Radboud University Medical Center, Radboud Institute for Health Sciences, Orthopaedic Research Laboratory

P.O.Box 9101, 6500 HB Nijmegen, The Netherlands

University of Twente, Department of Biomechanical Engineering

P.O.Box 217, 7500 AE Enschede, The Netherlands

---

[1] Corresponding author

Mailing address: P.O.Box 9101, 6500 HB Nijmegen, The Netherlands

Telephone: +31 (0)24 361 73 79

e-mail: Marco.Marra@radboudumc.nl

38   Nico.Verdonschot@radboudumc.nl

40 **ABSTRACT**

42 *Knowing the forces in the human body is of great clinical interest and musculoskeletal models are the most*

commonly used tool to estimate them in vivo. *Unfortunately, the process of computing muscle, joint*

44 *contact and ligament forces simultaneously is computationally highly demanding. The goal of this study*

was to develop a fast surrogate model of the tibiofemoral (TF) contact in a total knee replacement (TKR)

46 *model and apply it to force-dependent kinematic simulations of activities of daily living (ADLs). Multiple*

domains were populated with sample points from the reference TKR contact model, based on reference

48 *simulations and design-of-experiments. Artificial neural networks learned the relationship between TF*

pose and loads from the medial and lateral sides of the TKR implant. Normal and right-turn gait, rising-

50 *from-a-chair, and a squat were simulated using both surrogate and reference contact models. Compared*

to the reference contact model, the surrogate contact model predicted TF forces with a root-mean-square

52 *error (RMSE) lower than 10 N and TF moments lower than 0.3 Nm over all simulated activities. Secondary*

knee kinematics were predicted with RMSE lower than 0.2 mm and 0.2 degrees. Simulations that used the

54 *surrogate contact model ran on average three times faster than those using the reference model, allowing*

the simulation of a full gait cycle in 4.5 min. This modeling approach proved fast and accurate enough to

56 *perform extensive parametric analyses, such as simulating subject-specific variations and surgical-related*

factors in TKR.

58

60 **KEYWORDS**

64 **INTRODUCTION**

66   The calculation of forces acting on the musculoskeletal (MS) system during

activities of daily living (ADLs) is of great interest as it aids in understanding how hard

68 and soft tissues interact throughout the human body and at the joint level, and may

help researchers and clinicians to understand better the mechanical pathways of MS

70 pathologies. Body-level forces and moments are solved using multi-rigid body dynamic

methods, which are normally inexpensive computationally: given a known motion and

72 the external forces acting on the body, muscle and joint forces can be calculated by

means of forward dynamics assisted data tracking and inverse dynamics with

74 optimization-based muscle recruitment. The reader is referred to ref. [1] for an

extensive review of these techniques. At the joint and tissue level, more advanced

76 techniques – such as finite-element (FE) or elastic-foundation (EF) analyses – are

required to represent the contact interactions between articulating surfaces and solve

78 for ligament forces and secondary motions of the joints.

       Despite its great appeal, the coupling of such techniques for solving tissue-level

80 and body-level mechanics is overall a highly computationally demanding process, up to a

point that may hinder its clinical applicability or impede parametric and/or optimization

82 analyses on a large scale. Recently, the force-dependent kinematic (FDK) method [2]

was applied to estimate leg muscle forces, knee ligament and contact forces and

84 secondary kinematics simultaneously in a MS model of a patient having a total knee

replacement (TKR) [3]. However, the computational burden in that study was

86 considerable, as it took more than four hours to analyze a single cycle of normal gait.

Surrogate models have been proposed to reduce the computational burden of

88   MS simulations while retaining a reasonable level of accuracy. Halloran et al.

demonstrated adaptive surrogate modeling techniques to accelerate the optimization of

90   a jump height in a combined MS-FE model of the foot [4]. Surrogate models for the

analysis of native knee joint forces [5,6], cartilage stresses [7] and tibiofemoral (TF)

92   contact interactions and wear in total knee replacement (TKR) [8–11] were also

reported. These models utilized a variety of techniques, such as response surface

94   optimization [6], Lazy Learning [4], nonlinear dynamic models [5], Kriging [8–10], and

artificial neural networks (ANN) [5,7,11]. Recently, Eskinazi and Fregly (2015) proposed a

96   surrogate modeling approach based on ANN to accelerate an FE deformable contact

model of TKR [11]. Artificial neural networks are known, among others, for their ability

98   to learn virtually any complex relationship between a set of input and output variables

[12]. For instance, for the knee joint, one would train ANNs using outcomes of repeated

100   contact analyses of expensive reference FE or EF models, and subsequently fit the

relationships between TF pose and the resultant TF contact forces and moments. Then,

102   within a musculoskeletal analysis, the surrogate model would replace the reference

contact model, providing a significant reduction in computation time. However, the

104   performance of surrogate contact models for the simultaneous estimation of muscle

forces, TF ligament and contact forces and secondary kinematics during activities of

106   daily living (ADLs) has not been demonstrated yet.

The aim of this study is to create and test a surrogate contact model of a TKR and

108   to demonstrate its applicability in predicting muscle, ligament and TF contact forces and

secondary kinematics simultaneously during normal gait, right-turn gait, rising-from-a-

110 chair, and squat. We addressed the following specific questions: 1) how much reduction

in simulation time is obtained and 2) how well is accuracy retained when a surrogate

112 contact model is used instead of the reference contact model?

114 **METHODS**

116   A previously validated patient-specific MS model of a patient with a telemetric

knee prosthesis was the basis for this study [3]. The model was built using the AnyBody

118 Modeling System (AMS, version 6, AnyBody Technology A/S, Aalborg, Denmark) [13] and

included head, two arms, trunk, pelvis and two legs. Further details can be found in ref.

120 [3]. The analysis workflow consisted of two stages: a motion optimization (MO) and

force-dependent kinematics (FDK), which applies inverse dynamic analysis as part of the

122 solution process. In the first stage (MO), the full-body model was driven using marker

trajectories from motion-capture data, and joint kinematics were optimized using an

124 inverse kinematic analysis [14]. The AMS applies a full Cartesian formulation in which

each body is described by the translation of the segment origin and the segment

126 orientation specified with Euler parameters. The relative movement between the

segments is restricted by constraint equations, which, in this case, allowed three

128 translation and three rotations of the pelvis segment relative to the global reference

frame, three pelvis-trunk rotations, neck extension and for each leg, three hip rotations,

130 knee flexion, ankle plantarflexion and subtalar eversion. In the second stage (FDK), the

optimized joint kinematics from MO stage and the experimental ground reaction forces

132   and moments (GRF&Ms) were input to an FDK model, which solved for the 166 Hill-type

muscle element forces spanning the lower extremity, TF ligament and contact forces,

134   and secondary TF joint kinematics under an assumption of quasi-static equilibrium

within the joint [2]. To save computation time, the right (unaffected) leg and both arms

136   were excluded from the FDK analyses and artificial reaction forces and moments were

added to the pelvis segment to compensate for kinematic-kinetic inconsistencies.

138

Description of the Reference Contact Model

140

The reference TKR contact model of a left knee used in this study was extracted from

142   the aforementioned MS model. It consisted of two contact pairs defined by the femoral

component and the medial and lateral side of the tibial insert, respectively. Implant

144   geometries were obtained from the 5th "Grand Challenge Competition to Predict In Vivo

Knee Loads" dataset [15]. TF contact forces and moments were calculated using a linear

146   pressure-overclosure relationship between the articulating surfaces, in which the

contact forces were a linear function of the penetration volume, with a factor (pressure

148   modulus) of 9.3 GN/m³ [3].

To generate a surrogate contact model of TKR, it was necessary to find the

150   relationship between contact forces and moments resulting from the relative pose

between the tibial and femoral component. For this, we used a design-of-experiment

152   approach to define a model sampling scheme to obtain the desired input-output

relations. Subsequently, we fitted the samples obtained from repeated evaluation of the

154   reference contact model using ANN until convergence criteria were reached. Details of

this procedure are herein provided.

156   The tibial component, consisting of medial and lateral contact surfaces, was fixed

to the global reference frame. The femoral component was free to move in space having

158   6 DOFs relative to the global frame. Thus, the relative TF pose could be defined by three

translations and three rotations between tibial (fixed) and femoral (moving) frames of

160   reference (Fig. 1). Tibiofemoral translations were defined as the translations of the

femoral component frame measured with respect to the tibial frame of reference, and

162   corresponded to anterior femur translation (x), joint distraction (y), and medial femur

translation (z), respectively. Tibiofemoral rotations were defined using Tait-Bryan angles

164   with the 'z-y-x' sequence of intrinsic rotations from the femoral component body frame

to the tibial component body frame. This rotation sequence allowed the description of

166   knee abduction (ϑ_x) around a well-defined axis fixed in the tibial body. As will become

clearer in the next section, knee abduction was a sensitive rotation, therefore, it was

168   allowed to vary according to the abduction torque applied. Letting knee abduction be

the last rotation in the sequence, a change in the rotation did not affect the remaining

170   two non-sensitive rotations (ϑ_z and ϑ_y). Please note that the used sequence ('z-y-x'

rotations from femur to tibia) is equivalent to a 'x-y-z' rotation sequence from tibia to

172   femur, as defined in ref. [11], with an opposite sign convention. Furthermore, the

assumptions of conservative (friction-less) and linear elastic contact were made. Under

174   these conditions, it was possible to simplify the contact formulation and assume the

contact forces and moments to depend purely on TF pose. Tibio-femoral forces and

176   moments resulting from medial and lateral contact analyses were measured with

respect to the origin of the femoral coordinate system and expressed in the tibial

178   reference frame. They will be referred to as F_x^{Med}, F_y^{Med}, F_z^{Med}, M_x^{Med}, M_y^{Med}, M_z^{Med}, for

the medial side, and F_x^{Lat}, F_y^{Lat}, F_z^{Lat}, M_x^{Lat}, M_y^{Lat}, M_z^{Lat}, for the lateral side, in which the

180   subscripts indicate the direction of application of the load. The resultant forces and

moments from the medial and lateral sides combined could be conveniently expressed

182   as the total TF loads: F_x^{Tot}, F_y^{Tot}, F_z^{Tot}, M_x^{Tot}, M_y^{Tot}, M_z^{Tot}.

184   **Sampling of the Reference Contact Model**

186   An efficient sampling plan was necessary to ensure coverage of the design space.

Ideally, the surrogate model should have a perfect fit in all areas of the design space,

188   which are likely to occur in a simulation, and also adequate in less probable areas, in

order to prevent the contact algorithm from producing unacceptably large prediction

190   errors. Due to the particular geometry of the articulating surfaces in TKR, there are

specific directions in which minimal variations of the TF pose induce very large

192   variations in the corresponding TF loads. These are referred to as 'sensitive directions'

[8]. To identify possible sensitive directions in our contact model, we configured a

194   reference TF pose in which all rotations and the anterior and medial femur translation

were null and the femoral component "just touched" the tibial component.

196   Subsequently, we perturbed the TF pose and analyzed the TF load response. We

identified two sensitive directions, being the joint distraction (y) and the knee abduction

198   (ϑ_x), respectively. The presence of sensitive directions suggested a definition of sample

points as combinations of pose parameters in non-sensitive directions and loads in

200   sensitive directions: $\{x, F_y^{Tot}, z, M_x^{Tot}, \vartheta_y, \vartheta_z\}$, as in [8]. This definition was adopted to

sample two-sided contact and contact boundary cases. To ensure a wider coverage of

202   the design space, one ought to include also out-of-contact and single-sided contact

cases [11]. In such cases, we adopted different definitions of the sample point, namely

204    $\{x, y, z, \vartheta_x, \vartheta_y, \vartheta_z\}$ for out-of-contact cases, for which the femoral component could be

freely moved far away from the tibial insert, and $\{x, F_y^{Tot}, z, \vartheta_x, \vartheta_y, \vartheta_z\}$ for single-sided

206   contact cases, for which the knee abduction angle could be explicitly prescribed so as to

produce lift-off on either sides, as in [11].

208   To define reasonable boundaries for the design space, we estimated and

extracted TF load-pose data from five reference FDK analyses of ADLs obtained using

210   our MS model with the reference contact model. These activities included one walking

cycle of normal gait, one of right-turn gait, an unloaded leg-swing, two repetitions of a

212   rising-from-a-chair task, and four repetitions of a squatting motion, for which motion-

capture data were available as part of the Grand Challenge dataset [15]. Differently than

214   in the study of Eskinazi and Fregly [11], in which reference curves were extracted from

14 gait cycles, we included reference curves from several types of ADLs, with the aim of

216   generalizing the capabilities of the surrogate contact model for future use, as we plan to

apply the surrogate model in MS analyses involving different loading conditions and

218   ranges of motion.

To take into account different contact cases, we adopted a multi-domain

220   approach, as in the study of Eskinazi and Fregly [11], and we chose the Hammersley

quasi-random (HQ) sequence [16] to evenly distribute points in each domain (Table 1).

222   However, some different choices were made for distributing samples points across

domains, as detailed below. By using multiple domains, we attempted to maximize the

224   coverage of areas of the design space that are as likely to occur as normal two-sided

contact during the analysis of ADLs, for instance including lift-off of one or both of the

226   two sides of the implant, or situations where the implant surfaces are barely in contact.

Domain 1 consisted of data points spanning the boundaries of ± 1 standard deviation

228   (SD) from the time-varying envelopes of each of the aforementioned reference analyses.

This domain compared to domains D1 and D2 in the study of Eskinazi and Fregly [11],

230   with the differences being the expansion factor of 1 SD (our method) as opposed to

20 % and 100 % (their method), and the fewer points sampled. For each time-frame, 20

232   data points were sampled, resulting in 18060 points. Our Domain 2 was comparable to

domain D3 in ref. [11], though the sampling process was different. We first performed a

234   principal component analysis (PCA) of the reference data, then we enlarged the

envelopes of the principal components (PCs) by 50 % and we sampled data points in the

236   new PC space. Finally, we transformed the PC samples back to the original variables

space. By pre-transforming the domain space using PCA, the resulting samples points

238   were more densely distributed around the data points of the reference curves. This

domain enlarged substantially the coverage with respect to the Domain 1, while still

240   retaining the gross inter-variability between the sampling variables, owing to PCA pre-

transformation. Domain 3 represented single-sided contact, similarly to domain D4 in

242   ref. [11], which simulated lift-off of one of the two sides of the implant. The sampling

point was defined as $\{x, F_y^{Tot}, z, \vartheta_x, \vartheta_y, \vartheta_z\}$. Differently than in ref. [11], the PCA approach

244   was used for the TF pose parameters and an upper boundary equal to 100 N was set on

F_y^{Tot} (lower boundary was 0 N), which covered situations with low contact forces on

246   either sides. Domain 4 consisted of contact boundary points, similar to domains D6 and

D7 in ref. [11], in which one or both sides were barely touching. This domain accounted,

248   for instance, for situations in which the leg would enter the swing phase of gait, and the

TF loads would progressively decrease. The sample point definition for this domain was

250     $\{x, F_y^{Tot}, z, M_x^{Tot}, \vartheta_y, \vartheta_z\}$, thus we set an upper boundary of 100 N on F_y^{Tot}, and a lower

and upper boundary of ± 5 Nm on M_x^{Tot}. This choice differed from that of Eskinazi and

252   Fregly for domain D6 and D7, in which the medial and lateral vertical contact forces

were kept fixed at 5 N, simultaneously or alternately, while sampling the TF pose

254   parameters. Domains 5 and Domain 6 were populated with samples representing both

sides out-of-contact cases, in which the femoral component was in the proximity

256   (Domain 5) and far away (Domain 6) from the tibial insert, respectively. The sample

point definition was $\{x, y, z, \vartheta_x, \vartheta_y, \vartheta_z\}$. Our Domain 5 was comparable to domain D5 in

258   ref. [11], but we sampled a much larger number of points. In this domain, the contact

boundary samples were re-used, and the distraction was raised up to 2 mm in four

260   increments (as opposed to three in ref. [11]). Furthermore, we extended the out-of-

contact coverage with Domain 6, to ensure that the response of the surrogate model did

262   not diverge dramatically when the femoral component separated substantially from the

tibial component, providing additional robustness to the surrogate model. In Domain 6,

264   boundaries on the *y* translation were set between the maximum *y* translation of contact

boundary cases and 10 cm.

266   All sample points were evaluated by repeated static analyses using the reference

contact model (Fig. 1), to obtain the combinations of TF pose and corresponding TF

268   loads. As for Domains 5 and 6 – in which samples consisted purely of pose parameters –

the analysis was displacement-driven and TF loads solved for using ordinary inverse

270   dynamics. Sampling domains that included sensitive directions for certain loads

(Domains 1-to-4) were analyzed using a combination of displacement-driven and force-

272   driven analyses, where TF pose parameters in non-sensitive directions and loads in

sensitive directions were prescribed, whereas TF pose parameters in sensitive directions

274   and loads in non-sensitive directions were simultaneously solved for using FDK analyses.

In these cases, the FDK algorithm solved for the unknown TF pose parameters in

276   sensitive directions that put the system in static equilibrium, under the application of TF

loads in sensitive directions and the prescribed pose in non-sensitive directions. Errors

278   of up to 0.1% of the applied loads were tolerated, whereas samples that led to larger

errors were discarded. Additionally, samples that led to TF component overclosure

280   larger than 2 mm were also filtered out. Approximately 85% of all the successful sample

points were allocated for surrogate model training. The remaining 15% were assigned to

282   a separate testing dataset. No samples were allocated for testing in Domain 1, as the

accuracy in this sort of domain would be better evaluated by FDK analysis of ADLs.

284

Training of the Surrogate Contact Model

286

Multiple-input multiple-output feedforward ANNs were configured in MATLAB (version

288   8.6.0, The MathWorks Inc., Natick, MA) using the Neural Network Toolbox (Fig. 2). As

opposed to the study of Eskinazi and Fregly, who interconnected multiple ANNs, each

290   with multiple inputs and a single output [11], we opted for ANNs with multiple inputs

and multiple outputs in an attempt to exploit the correlation likely to exist between

292   different output variables. Similarly to ref. [11], the training phase consisted of two

stages: in the first stage, one ANN learned the relationship between medial and lateral

294   TF loads in sensitive directions, $\{F_y{}^{Lat}, M_x{}^{Lat}, F_y{}^{Med}, M_x{}^{Med}\}$, and the TF pose, $\{x, y, z, \vartheta_x, \vartheta_y,$

$\vartheta_z\}$; in the second stage, two additional ANNs learned the relations between the

296   remaining medial and lateral TF loads separately, and a combination of TF pose

parameters and sensitive loads of either side. This allowed proper learning of the out-of-

298   contact cases, in which zero loads may correspond to many different combinations of

pose parameters and to have fully independent medial and lateral surrogate contact

300   models.

Given the impossibility to establish *a priori* the correct number of layers and

302   neurons, a heuristic method was used to decide both number of network layers and

neurons per layer. We started with two hidden layers and ten neurons per layer. We

304   started the network training and recorded the value of the performance function after

one hour. If the performance value fell below 0.001, then we would accept the current

306   network configuration, else we would primarily add ten neurons to each layer (up to

forty neurons in total per layer) and, secondly, add one more hidden layer. After each

308   network modification we would repeat the one-hour training test. This process led us to

a final network configuration consisting of three hidden layers with thirty neurons per

310   layer, having hyperbolic tangent sigmoid transfer function. The network was then

completed with one output layer of purely linear neurons.

312   Each network was trained using the MATLAB training function `trainbr`, which uses Bayesian regularization within the Levenberg-Marquardt backpropagation

314   algorithm. According to this training scheme, the performance function to be minimized was a linear combination of squared errors and weights, in which the coefficients were

316   continuously updated to prevent data over-fitting and lead to networks with good generalization qualities. Each network trained for at least 18 hours and the training was

318   stopped only after the performance function visibly converged.

        After training succeeded, the weights and biases of each network were exported

320   as standalone functions using built-in MATLAB capabilities. Custom-written MATLAB routines translated those standalone functions into C++ code. The Eigen template library

322   [17] was used to represent and operate on numerical data in the C++ surrogate model functions. The latter were then built together as a dynamic-link library (DLL) to maximize

324   efficiency. A post hoc condition was defined in the surrogate model functions: if the medial or lateral TF force in the *y* direction was negative or equal to zero, then all

326   remaining loads on the respective side were immediately assigned zero as well, without calculating the output of the second stage.

328

Testing of the Surrogate Contact Model and Performance of Simulated ADLs

330

We used the surrogate contact model functions to evaluate the sample points from the

332   testing dataset, and reported the testing performances using the coefficient of determination (R^2, defined by 1 - sum of squares of residuals divided by total sum of

334   squares) and the root-mean-square error (RMSE) of output medial and lateral TF loads relative to targets.

336   We then replaced the reference contact model of the MS model with the newly

built surrogate contact model. This was achieved using C++ hook capabilities of the

338   AMS, which can load external DLL functions and make them available to the model

during run time. In this way, the medial and lateral TF contact loads were obtained by

340   executing function calls to the respective medial and lateral surrogate model DLL

functions, using the current TF pose as input argument. Differently from our previous

342   MS model [3], in which the computation of muscles and ligament lines of action – or

wrapping algorithm – was carried out using numerical methods, in this study, we opted

344   for an analytical solution[2], to prevent possible hindrances to the true performances of

the surrogate model. Moreover, since we were interested in testing a surrogate model

346   of a TKR TF joint, we replaced the patellofemoral (PF) joint with an ideal revolute joint

and let the only DOF of patella be controlled by an elastic patellar ligament (stiffness

348   1187 N/mm). During an analysis, the FDK algorithm explored the TF pose space until a

quasi-static equilibrium was reached, and to do so it iteratively executed function calls

350   to the surrogate model, rather than executing function calls to the reference contact

model. To evaluate the performance of the surrogate contact model for the analysis of

352   dynamic motor tasks, we simulated four ADLs using both the reference and the

surrogate contact model. We simulated one walking cycle of normal gait, one of right-

354   turn gait, two repetitions of a rising-from-a-chair task, and four repetitions of a

squatting motion for which motion capture data were available as part of the Grand

356   Challenge dataset [15]. For each activity and for each contact model, we estimated TF

---

[2] The algorithm for the analytical solution is not part of the AMS release and it was provided separately to us by AnyBody Technology A/S in a prototype version that solved a single cylindrical wrapping case.

forces, moments and six-DOF knee kinematics and we evaluated the accuracy of the

358   surrogate model predictions compared to the predictions obtained with the reference

model. We calculated R^2, RMSE, and maximum prediction errors for all TF forces,

360   moments, and kinematics. Knee kinematics were defined according to a knee joint

coordinate system consistent with the description of Grood and Suntay [18].

362   Tibiofemoral rotations were defined using Tait-Bryan angles with the 'z-x-y' sequence of

intrinsic rotations from the femoral component body frame to the tibial component

364   body frame. Note that this convention differed from that used during the sampling

process; however, this choice was justified to provide a physically meaningful

366   description of knee kinematics; namely, anterior tibial translation, joint distraction,

lateral tibial translation, knee flexion, knee adduction, and tibial external rotation.

368   Additionally, we compared the computation times required to complete the FDK

analyses with either contact model.

370

RESULTS

372

On the testing dataset, the surrogate model predicted medial and lateral TF

374   loads with an R^2 value greater than 0.99 and 0.96, respectively, for all components of

force and moment. The largest medial and lateral RMS force errors (Table 2) were

376   observed in F_y^{Lat} (76 N, Domain 6) and F_y^{Med} (20 N, Domain 3), respectively. The largest

medial and lateral RMS moment errors were observed in M_x^{Med} (0.72 Nm, Domain 6)

378   and M_x^{Lat} (1.9 Nm, Domain 6). Maximum errors were in most cases one to two orders of

magnitude larger than RMS errors, indicating the presence of extreme outliers. The

380 largest maximum errors were 1863 N in $F_y{}^{Lat}$ and 50 Nm in $M_x{}^{Lat}$, both found on

Domain 2.

382   On the simulations of normal gait, right-turn gait, rising-from-a-chair, and squat,

medial and lateral TF loads were predicted with an R^2 value greater than 0.99 and 0.98

384 in all cases. The knee kinematics obtained with the surrogate model agreed to those

obtained with the reference model with an R^2 value greater than 0.96 in all cases,

386 except for lateral tibial translation in the normal gait ($R^2 = 0.93$). The largest RMS errors

among all trials (Table 3) were 5.6 N in $F_y{}^{Med}$ and 9.9 N in $F_y{}^{Lat}$, and 0.17 Nm in $M_x{}^{Med}$ and

388 0.26 Nm in $M_x{}^{Lat}$. The largest maximum errors on TF loads were 47 N for $F_y{}^{Lat}$ in the

right-turn and 1.4 Nm for $M_x{}^{Med}$ in the normal gait. The largest RMS errors in knee

390 kinematics (Table 4) were found in lateral tibial translation (0.13 mm) and tibial external

rotation (0.17 degrees) in the right-turn. Maximum errors reached up to 0.90 mm for

392 anterior tibial translation and up to 1.27 degrees for tibial external rotation, both in the

right-turn.

394   Simulation times (Table 5) were 4.5 and 13.6 min for the normal gait, 7.3 and

22.7 min for the right-turn trial, 27.2 and 70.3 min for the rising-from-a-chair trial, and

396 38.5 and 96.4 min for the squat trial, when using the surrogate and reference contact

model, respectively. The speed improvement introduced by the surrogate model was

398 greater than 2.5 times for the squat and rising-from-a-chair trials, and greater than 3

times for the normal gait and right-turn trials, thus it was greatest in trials with a short

400 duration and a fewer number of time frames analyzed (less than 2 s/200 frames), as

opposed to trials with a longer duration (more than 8 s/1000 frames).

402

DISCUSSION

404

In this study, we successfully incorporated a surrogate contact model of a TKR

406 based on ANNs into a MS model that solved for lower extremity muscle, TF ligament and

contact forces and secondary TF kinematics simultaneously. Tibiofemoral contact forces

408 and moments and secondary kinematics were predicted almost as accurately as with the

reference contact model in all ADLs, but within a third of the time. The ability to reduce

410 the computation time of MS analyses is an important step forward towards the

application of MS models in extensive parametric studies and/or the planning of

412 orthopedic interventions through optimization.

The prediction errors remained low across the different ADLs analyzed and

414 among different components of the loads. For instance, RMS errors on TF compressive

forces were on average less than 1% of peak forces reported for gait [19]. The RMS and

416 maximum errors were lower than 10 N/0.26 Nm and 47 N/1.4 Nm for all load

components, respectively. The sampling scheme based on multiple domains proved thus

418 effective in providing a good coverage for the contact conditions arising during the ADLs

simulated.

420 The RMS errors for the prediction of TF contact forces and moments during gait

simulations (1.9 N/0.063 Nm) were on the same order of magnitude but slightly lower

422 than the errors reported by Eskinazi and Fregly (2.6 N/0.078 Nm) [11]. Sub-millimeter

and sub-degree accuracy was also achieved in predictions of secondary knee kinematics

424 in all ADLs investigated, indicating that the iterative process that computed the quasi-

static equilibrium in the secondary knee DOFs converged to very similar results.

426 Moreover, when the goal is to capture the overall kinematics for various ADLs, as was in

the current study, small errors in the TF loads predicted by the surrogate model do not

428 critically affect the kinematic results of the simulations. None of the previous studies

reported on the accuracy of secondary knee kinematics predicted concurrently with

430 muscle, ligament and contact forces using a surrogate TF contact model.

The time to complete an FDK analysis of the ADLs investigated in this study was

432 reduced by about three times when the surrogate contact model replaced the reference

contact model. The speed improvement appeared quite modest and warranted further

434 exploration. To exclude possible hidden overhead within the surrogate model functions,

we investigated the execution time of isolated surrogate contact model function calls:

436 this was on the order of 77 μs per evaluation, as opposed to 78 ms for the reference

contact model. Thus, at the level of isolated function calls, the surrogate model was

438 about 1000x faster than the reference contact model, as expected, however such a

speed improvement did not extend to FDK analyses of ADLs. This can be explained by

440 other time-consuming processes taking place within such analysis; namely, the

kinematic analysis, and the optimization that solved the muscle recruitment problem.

442 Both processes were solved numerically using iterative algorithms which themselves

added overhead. Replacing the reference contact model with a faster surrogate contact

444 model removed a part of this overhead.

A full gait cycle could be analyzed in just 4.5 min, using a surrogate contact

446 model, which is of practical advantage in many cases. Extensive parametric studies often

require repeating similar analyses hundreds or thousands of times to assess the

448   influence of individual parameters. For instance, it could be interesting to study the

performances of a certain implant design under varying subject-specific factors, such as

450   height, weight, muscle strength, soft tissue characteristics, and limb alignment and/or

implant related factors, such as implant alignment. In all these cases, very low

452   computation times would be highly beneficial, as it would eliminate an important

bottleneck in the implementation of such analyses.

454   The simulation time to analyze one walking cycle of normal gait (4.5 min) was

almost one order of magnitude smaller than the time reported by a previous study that

456   used surrogate contact models of both TF and PF joints (42 min) [9]. Our model did not

include a PF joint contact model; however, it included 166 Hill-type muscles elements

458   spanning the entire lower extremity, in addition to TF ligaments and contact forces, as

opposed to the other study, which included only eleven muscles spanning the knee joint

460   and omitted all knee ligaments except the patellar ligament [9]. Other studies which did

not employ surrogate models reported simulation times to complete a forward and

462   inverse dynamic analysis of one walking cycle which were comparable to ours (a few to

ten minutes) [20–22]. However, these models did not include muscles and some

464   motions were input to the simulations; namely, knee anterior-posterior translation and

internal-external rotation. The analysis approach of the present study solved for the

466   muscle forces of the entire lower extremity and did not prescribe any of the secondary

knee kinematics. We believe that estimating muscle, ligament and joint contact forces

468   and secondary knee kinematics simultaneously – rather than prescribing or neglecting

any of them – is essential if the aim is to investigate the effect of implant-related factors

470   on the overall joint function, as any of the aforementioned outcomes may affect and/or

be affected by the different implant conditions. Thus, when the higher computational

472   complexity of our modeling approach is taken into account, the time performances

appear more than justified.

474   When evaluating the surrogate model over a testing dataset, RMS prediction

errors were all lower than 76 N (F_y^{Lat} on Domain 6) and 1.9 Nm (M_x^{Lat} on Domain 6). The

476   presence of extreme outliers was also noted, as testified by maximum errors in certain

domains that were orders of magnitude higher than the RMS errors in those domains:

478   1863 N for F_y^{Lat} and 50 Nm for M_x^{Lat}, both on Domain 2. This signifies the presence of

tiny areas of the design space that the surrogate model could not learn accurately

480   enough and for which it produced large errors. This could have happened if, for

instance, too few sample points were available in those areas during training of the

482   surrogate model, resulting in large testing errors, or if an insufficient number of hidden

layers was used in the ANN. A careful inspection of the 'problematic' points revealed

484   that the corresponding pose parameters referred to non-physiological situations, with

the femoral component almost below the tibial insert and/or rotated to a very large

486   extent. Such cases are very unlikely encountered in realistic contact situations, and,

therefore, they should not constitute a serious problem. If we exclude from the

488   comparison our Domain 6, which does not have an analogous in a previous study [11],

then the largest errors were found on analogous domains in both studies; namely, our

490   Domain 2 and their domain 'D3', which represented an expansion of the global

reference curves. In these analogous domains, the largest RMS (maximum) errors in our

492   study were 69 N/1.8 Nm (1863 N/50 Nm) as opposed to 14 N/0.4 Nm (249 N/4.7 Nm) in

[11]. Thus, our RMS (maximum) errors were up to five (ten) times larger, which could be

494   due to the different sampling choices (we used an expansion factor that was twice as

large) and/or different surrogate model architectures.

496   A surrogate contact modeling toolbox (SCMT) for the creation of surrogate

contact models was recently presented and made freely available by Eskinazi and Fregly

498   [23]. This toolbox was tested for the replacement of an EF contact model of both TF and

PF joints in a TKR model. In this study, we developed our own surrogate model creation

500   process, as the reference contact model of TKR was already available, as part of a

previously published MS model validated against knee forces and kinematics [3].

502   Furthermore, the previously published toolbox could not easily connect to our modeling

environment, which let us pursue the development of a dedicated surrogate model

504   creation process.

        Our surrogate modeling approach introduced some novel aspects, as compared

506   to previous studies, which are worth discussing. First, an advantage of the used FDK

approach is that it eliminates the sensitivity of predicted muscle, ligament, and joint

508   contact forces to errors in the location of a fixed knee flexion-extension axis when such

is assumed in the applied knee model. When a fixed knee flexion-extension axis is used,

510   typically only muscle forces are assumed to contribute to the net joint moment about

the fixed axis, whereas the contribution from contact and ligament forces are neglected.

512   Using FDK, the joint DOFs are left free to equilibrate under the compound action of

muscle, ligaments and contact forces (in a quasi-static fashion) and no assumptions are

514   required about the DOFs to which contact (and ligament) forces do not, and do,

contribute. This methodology relieves very much the efforts when modeling complex

516   non-conforming joints, such as the knee [2]. Second, pre-transforming the sampling

variables using PCA in Domain 2 and Domain 3 likely made our sampling scheme more

518   efficient, as the resulting sample points could be more densely distributed close to the

data points from the reference curves. This is due to the PCA being able to decouple the

520   original variables, thus allowing sampling along the principal directions of the reference

data points. Third, although an explicit comparison was not performed in this study,

522   choosing multiple-output instead of single-output ANNs may have benefitted the final

accuracy, as the covariance existing between the output loads was taken into account

524   during the fitting process, whereas single-output ANNs would fit each of the output

variables independently from the others. However, this should be investigated in a

526   future study. Fourth, using Bayesian regularization as part of the ANN training algorithm

helped preventing data over-fitting and producing ANNs with good generalization

528   qualities. Using a training algorithm that does not intrinsically over-fit the data has also

the practical advantage of not requiring a constant monitoring of the training state

530   and/or an additional dataset on which to perform validation.

We should note that our surrogate model creation process is not limited

532   uniquely to the contact model presented in this study, but can be easily extended to

virtually any other FE or EF contact models, provided that the assumptions of elastic and

534   friction-less contact are met. In that respect, the surrogate model could provide a fast

and valid alternative to contact models which cannot directly interface to the modeling

536   system of use. Furthermore, the surrogate model resulting from our creation process

can be exploited in virtually any simulation software capable of integrating an external

538   DLL module. This represents a very viable way to describe complex structural models,

without actually simulating them.

540   The time required to generate the sample points amounted to almost 5 days of

continuous computation on all four cores of an Intel® Core™ i5-4570 quad-core CPU

542   equipped with 16 gigabytes of RAM. About 60 additional hours were necessary to train

the ANNs. The total surrogate model generation time was considerable, however, both

544   the sampling process and the training of the neural networks could be massively

parallelized and executed on multiple processing units, or machines with many cores.

546   This approach would easily bring the generation time to more manageable levels. It

should also be noted that the generation time for a given implant design is paid only

548   once upfront, but the resulting surrogate model can be reused for the evaluations of

many conditions and multiple patients. Another way to reduce the generation time

550   would be to reduce the number of training points, but this aspect requires further

investigation.

552   The sample generation process relied heavily on reference curves and/or

variables bounds extracted from existing reference simulations performed with the

554   reference model. This approach may work well when such data are already available –

or if they can easily be obtained from experimental measurements – however, this is

556   seldom the case. Perhaps the most challenging case is that of a patient-specific knee

model, generated *ex novo* from medical images of the patient. In such a case, although

558   some joint kinematics may be extracted using *in vivo* imaging techniques, no reference

load curves are available and a different sampling strategy should be devised. The

560   definition of bounds for the sample points could also be based on the geometrical

conformity between the articulating surfaces, and bounds on joint loads in sensitive

562   directions could be obtained from the literature. However, these approaches require

further investigation.

564   The activities simulated in this study were also incidentally used during the

sampling stage to provide reference curves. If activities were to be simulated which

566   involved joint loads and/or kinematics very different from the ones in the training

dataset, it is almost impossible to know whether the surrogate model predictions would

568   still be sufficiently accurate. One possible solution could be to build accuracy maps over

various regions of the design space and, subsequently, to relate the distance of new

570   query points from the dataset of training points prior to the surrogate model evaluation

to estimate the expected accuracy for the new points. However, mapping the accuracy

572   over a multi-dimensional domain is not trivial.

We introduced a discontinuity in the surrogate model, which prevented negative

574   forces in the TF distraction (y) direction, and avoided the estimation of TF loads in non-

sensitive directions when the compressive force was lower than or equal to zero. To find

576   the configuration of static equilibrium in the TF joint, the FDK method solves a set of

nonlinear equations using gradient information. Therefore, our choice made the

578   gradient of the system of equations potentially discontinuous, whereas a smooth

transition to zero would be a better choice. However, the reference contact model

580   contained the same discontinuity and the surrogate contact model did not exacerbate

this problem.

582   Friction between the articular implant surfaces was neglected and the contact

was assumed to be linear elastic based on penetration volume. The friction-less

584   assumption may not allow proper study of polyethylene wear of the tibial insert under

dynamic conditions. However, for all other cases of interest (e.g., parametric variation,

586   knee kinematic studies and ligament force predictions), this assumption does not

represent a major limitation. With regards to the linear elastic assumption, previous

588   studies have failed to demonstrate the superiority of non-linear contact models over

linear models to describe the load response of the polyethylene component [24].

590   However, the surrogate contact model creation process should work just as well for

non-linear elastic contact models, as long as the contact forces and moments can be

592   represented as functions of only model pose.

In conclusion, we successfully applied surrogate modeling techniques based on

594   ANNs to reduce the computation time of knee joint loads and kinematics in MS models.

We evaluated its accuracy and demonstrated its performance in the simulation of four

596   ADLs. Accuracy was comparable to that of the reference model, while simulations were

performed three times as fast, with a full gait cycle analyzed in only 4.5 min. We believe

598   that these performances will promote the applicability of MS models in extensive

parametric studies and/or planning of orthopedic interventions through optimization.

600

602 **FUNDING**

612   **REFERENCES**

614   [1]   Erdemir, A., McLean, S., Herzog, W., and van den Bogert, A. J., 2007, "Model-based estimation of muscle forces exerted during movements.," Clin Biomech

616   (Bristol, Avon), **22**(2), pp. 131–54.

      [2]   Andersen, M. S., Damsgaard, M., and Rasmussen, J., 2011, "Force-dependent

618   kinematics: a new analysis method for non-conforming joints," XIII International Symposium on Computer Simulation in Biomechanics, Leuven, Belgium.

620   [3]   Marra, M. A., Vanheule, V., Fluit, R., Koopman, B. H. F. J. M., Rasmussen, J., Verdonschot, N., and Andersen, M. S., 2015, "A subject-specific musculoskeletal

622   modeling framework to predict in vivo mechanics of total knee arthroplasty.," J Biomech Eng, **137**(2), p. 20904.

624   [4]   Halloran, J. P., Erdemir, A., and van den Bogert, A. J., 2009, "Adaptive surrogate modeling for efficient coupling of musculoskeletal control and tissue deformation

626   models.," J Biomech Eng, **131**(1), p. 11014.

      [5]   Mishra, M., Derakhshani, R., Paiva, G. C., and Guess, T. M., 2011, "Nonlinear

628   surrogate modeling of tibio-femoral joint interactions," Biomed Signal Process Control, **6**(2), pp. 164–174.

630   [6]   Lin, Y.-C., Farr, J., Carter, K., and Fregly, B. J., 2006, "Response surface optimization for joint contact model evaluation.," J Appl Biomech, **22**(2), pp. 120–

632   30.

      [7]   Lu, Y., Pulasani, P. R., Derakhshani, R., and Guess, T. M., 2013, "Application of

634   neural networks for the prediction of cartilage stress in a musculoskeletal system.," Biomed Signal Process Control, **8**(6), pp. 475–482.

636   [8]   Lin, Y.-C., Haftka, R. T., Queipo, N. V, and Fregly, B. J., 2010, "Surrogate articular contact models for computationally efficient multibody dynamic simulations.,"

638   Med Eng Phys, **32**(6), pp. 584–94.

      [9]   Lin, Y.-C., Walter, J. P., Banks, S. A., Pandy, M. G., and Fregly, B. J., 2010,

640   "Simultaneous prediction of muscle and contact forces in the knee during gait.," J Biomech, **43**(5), pp. 945–52.

642   [10]   Lin, Y.-C., Haftka, R. T., Queipo, N. V, and Fregly, B. J., 2009, "Two-dimensional surrogate contact modeling for computationally efficient dynamic simulation of

644   total knee replacements.," J Biomech Eng, **131**(4), p. 41010.

      [11]   Eskinazi, I., and Fregly, B. J., 2015, "Surrogate modeling of deformable joint

646   contact using artificial neural networks.," Med Eng Phys, **37**(9), pp. 885–91.

      [12]   Hornik, K., Stinchcombe, M., and White, H., 1989, "Multilayer feedforward

648   networks are universal approximators," Neural Networks, **2**(5), pp. 359–366.

      [13]   Damsgaard, M., Rasmussen, J., Christensen, S. T., Surma, E., and de Zee, M.,

650   2006, "Analysis of musculoskeletal systems in the AnyBody Modeling System," Simul Model Pract Theory, **14**(8), pp. 1100–1111.

652   [14]   Andersen, M. S., Damsgaard, M., and Rasmussen, J., 2009, "Kinematic analysis of over-determinate biomechanical systems.," Comput Methods Biomech Biomed

654   Engin, **12**(4), pp. 371–84.

      [15]   Fregly, B. J., Besier, T. F., Lloyd, D. G., Delp, S. L., Banks, S. a, Pandy, M. G., and

656   D'Lima, D. D., 2012, "Grand challenge competition to predict in vivo knee loads.," J Orthop Res, **30**(4), pp. 503–13.

658   [16]   Hammersley, J. M., 2006, "MONTE CARLO METHODS FOR SOLVING MULTIVARIABLE PROBLEMS," Ann N Y Acad Sci, **86**(3), pp. 844–874.

660   [17]   Guennebaud, G., Jacob, B., and others, 2010, "Eigen v3" [Online]. Available: http://eigen.tuxfamily.org.

662   [18]   Grood, E. S., and Suntay, W. J., 1983, "A joint coordinate system for the clinical description of three-dimensional motions: application to the knee.," J Biomech
664   Eng, **105**(2), pp. 136–44.

   [19]   D'Lima, D. D., Fregly, B. J., Patil, S., Steklov, N., and Colwell, C. W., 2012, "Knee
666   joint forces: prediction, measurement, and significance.," Proc Inst Mech Eng H, **226**(2), pp. 95–102.

668   [20]   Bei, Y., and Fregly, B. J., 2004, "Multibody dynamic simulation of knee contact mechanics.," Med Eng Phys, **26**(9), pp. 777–89.

670   [21]   Fregly, B. J., Sawyer, W. G., Harman, M. K., and Banks, S. A., 2005, "Computational wear prediction of a total knee replacement from in vivo
672   kinematics.," J Biomech, **38**(2), pp. 305–14.

   [22]   Fregly, B. J., Banks, S. A., D'Lima, D. D., and Colwell, C. W., 2008, "Sensitivity of
674   knee replacement contact calculations to kinematic measurement errors.," J Orthop Res, **26**(9), pp. 1173–9.

676   [23]   Eskinazi, I., and Fregly, B. J., 2016, "An Open-Source Toolbox for Surrogate Modeling of Joint Contact Mechanics.," IEEE Trans Biomed Eng, **63**(2), pp. 269–77.

678   [24]   Fregly, B. J., Bei, Y., and Sylvester, M. E., 2003, "Experimental evaluation of an elastic foundation model to predict contact pressures in knee replacements.," J
680   Biomech, **36**(11), pp. 1659–68.

682

Table Caption List

Table 1   Sampling domains, number of samples and approximate sampling time for each domain

Table 2   RMS (maximum) prediction errors of medial (*Med*) and lateral (*Lat*) TF loads for the testing dataset in each sampling domain.

Table 3   RMS (maximum) prediction errors of medial (*Med)* and lateral (*Lat*) TF loads for normal gait, right-turn, rising-from-a-chair, and squat.

Table 4   RMS (maximum) prediction errors of knee kinematic parameters for normal gait, right-turn, rising-from-a-chair, and squat.

Table 5   Simulation times and speed improvement for surrogate vs. reference contact model for normal gait, right-turn, rising-from-a-chair, and squat.

Figure Captions List

Fig. 1   Contact model of TKR. The TF pose is defined by the relative translation

and rotation between the femoral component frame (blue) and the tibial

component frame (red). Tibiofemoral translations are expressed in the

tibial component frame of reference, and represent anterior femur

translation (x), joint distraction (y), and medial femur translation (z).

Tibiofemoral rotations are expressed in the femoral component frame of

reference with Cardan angles using the *z-y-x* sequence of rotations,

where the first rotation represent knee extension, the second, tibial

external rotation, and the third, knee abduction. Rigid surface contact

based on pressure-overclosure is defined between medial and lateral

side of tibial component and femoral component. To obtain samples for

the surrogate model, this contact model is evaluated using repeated

static analyses.

Fig. 2   Diagram of the 2-stage feedforward artificial neural network (ANN). The

stage I network (left) learned the relations between TF loads in sensitive

directions (F_y^{Med}, T_x^{Med}, F_y^{Lat}, T_x^{Lat}) and the TF pose parameters; in stage II

(right) the remaining TF loads of medial (lateral) side are obtained as

functions of the TF pose and the medial (lateral) TF loads from stage I.

HL: hidden layers, W: network weights, b: network biases.

Fig. 3   Medial (top) and lateral (bottom) TF compressive forces during normal

gait, right-turn, rising-from-a-chair, squat simulation. Reference measured force (eTibia, shaded), predictions using surrogate (solid) and reference (dotted) contact model.

Fig. 4   Anterior tibial translation, joint distraction, lateral tibial translation, knee flexion, knee adduction and tibial external rotation predicted using the reference contact model (solid line) and the surrogate contact model (dotted line) during normal gait, right-turn, rising-from-a-chair, and squat simulation.

688

Table 1

Domain	Description	Number of training samples	Number of testing samples	Approximate sampling time core time (effective time)[a]
1	Time-varying local envelopes of reference simulations expanded by 1 SD	18 060	-	102 (25) hours
2	Global envelopes of reference simulations expanded by 50 %	27 253	3 416	226 (57) hours
3	Single-sided contact (lift-off cases)	10 000	1 765	47 (12) hours
4	Contact boundary (swing phase)	9 990	1 755	70 (17) hours
5	Out-of-contact, proximity cases (y up to 2 mm, in four steps)	67 760	11 958	11 (3) hours
6	Out-of-contact, far away cases (y up to 10 cm, coarse)	2 000	353	15 (4) min
	Total	134 973	19 247	456 (114) hours

690   [a]Sampling time referred to a single CPU core. Considering a total of 4 cores per CPU, the effective sampling time is reduced by four.

692

Table 2

Domain	Side	F_x (N)	F_y (N)	F_z (N)	M_x (Nm)	M_y (Nm)	M_z (Nm)
2	Med	3.8 (58)	18 (462)	3.2 (32)	0.44 (9.7)	0.09 (1.4)	0.21 (6.5)
	Lat	12 (379)	69 (1863)	9.3 (315)	1.8 (50)	0.32 (11)	1.1 (41)
3	Med	3.9 (32)	20 (113)	6.8 (81)	0.46 (2.9)	0.14 (1.5)	0.21 (1.7)
	Lat	5.2 (48)	29 (191)	8.0 (126)	0.71 (5.3)	0.19 (2.3)	0.40 (6.7)
4	Med	2.1 (23)	9.9 (108)	3.9 (41)	0.26 (2.3)	0.07 (0.58)	0.12 (2.3)
	Lat	2.3 (14)	13 (77)	3.3 (49)	0.35 (2.3)	0.07 (0.51)	0.14 (1.1)
5	Med	0.13 (3.2)	1.0 (16)	0.44 (8.0)	0.03 (0.57)	0.01 (0.11)	0.01 (0.16)
	Lat	0.15 (5.3)	1.4 (25)	0.20 (5.4)	0.04 (0.42)	0.00 (0.21)	0.01 (0.15)
6	Med	8.4 (140)	17 (273)	3.2 (41)	0.72 (12)	0.13 (2.0)	0.02 (0.3)
	Lat	44 (602)	76 (1192)	51 (727)	1.9 (28)	1.8 (21)	0.77 (11)

694

696 **Table 3**

Trial	Side	F_x (N)	F_y (N)	F_z (N)	M_x (Nm)	M_y (Nm)	M_z (Nm)
Normal gait	Med	0.50 (2.2)	4.2 (14)	1.1 (11)	0.17 (1.4)	0.02 (0.09)	0.04 (0.17)
	Lat	0.50 (2.0)	4.4 (17)	0.43 (2.7)	0.12 (0.54)	0.02 (0.08)	0.01 (0.05)
Right-turn	Med	0.49 (3.0)	4.3 (24)	2.2 (11)	0.14 (0.65)	0.04 (0.18)	0.04 (0.16)
	Lat	0.95 (4.8)	9.9 (47)	2.2 (21)	0.26 (1.2)	0.03 (0.17)	0.10 (0.6)
Rising-from-a-chair	Med	0.85 (2.7)	5.6 (13)	0.51 (1.5)	0.11 (0.28)	0.01 (0.04)	0.06 (0.14)
	Lat	0.57 (2.0)	5.7 (13)	0.66 (2.1)	0.11 (0.30)	0.02 (0.07)	0.06 (0.16)
Squat	Med	0.34 (1.1)	4.2 (10)	0.51 (2.0)	0.10 (0.23)	0.01 (0.02)	0.06 (0.15)
	Lat	0.29 (0.96)	3.7 (11)	0.55 (2.2)	0.10 (0.23)	0.01 (0.04)	0.04 (0.13)

698

Table 4

| Trial	Anterior Tibial Translation (mm)	Joint Distraction (mm)	Lateral Tibial Translation (mm)	Knee Flexion (deg)	Knee Adduction (deg)	Tibial External Rotation (deg)
Normal gait	0.06 (0.34)	0.01 (0.06)	0.07 (0.15)	0.00 (0.00)	0.01 (0.06)	0.04 (0.30)
Right-turn	0.12 (0.90)	0.10 (0.62)	0.13 (0.84)	0.09 (0.43)	0.14 (0.72)	0.17 (1.27)
Rising-from-a-chair	0.03 (0.16)	0.01 (0.03)	0.01 (0.08)	0.01 (0.02)	0.01 (0.06)	0.03 (0.14)
Squat	0.02 (0.10)	0.00 (0.01)	0.00 (0.03)	0.00 (0.02)	0.01 (0.02)	0.03 (0.10)

700

702 **Table 5**

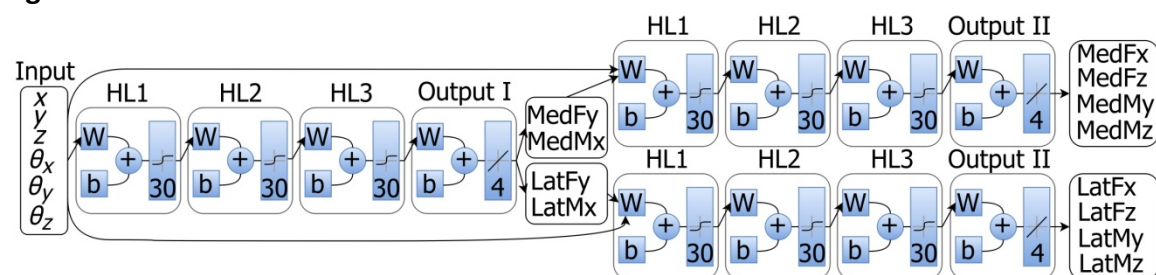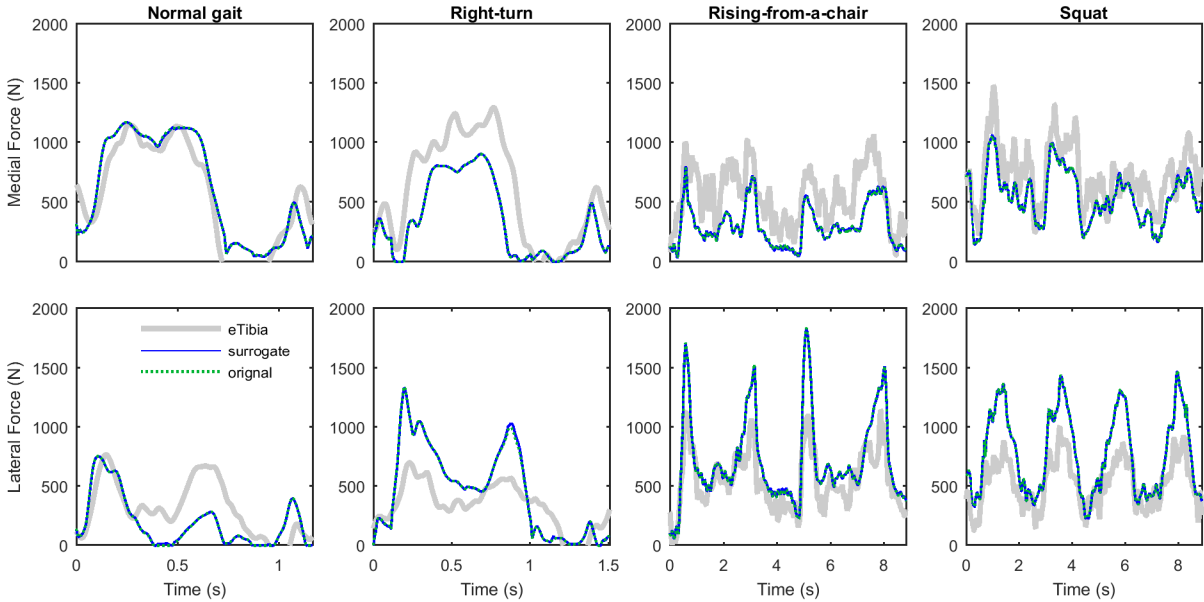| Trial	Number of time-frames	Trial duration (s)	FDK simulation time		Speed improvement
			Reference model (min)	Surrogate model (min)	
Normal gait	146	1.2	13.6	4.5	3.0
Right-turn	187	1.5	22.7	7.3	3.1
Rising-from-a-chair	1066	8.8	70.3	27.2	2.6
Squat	1074	8.9	96.4	38.5	2.5

704

Figure 1
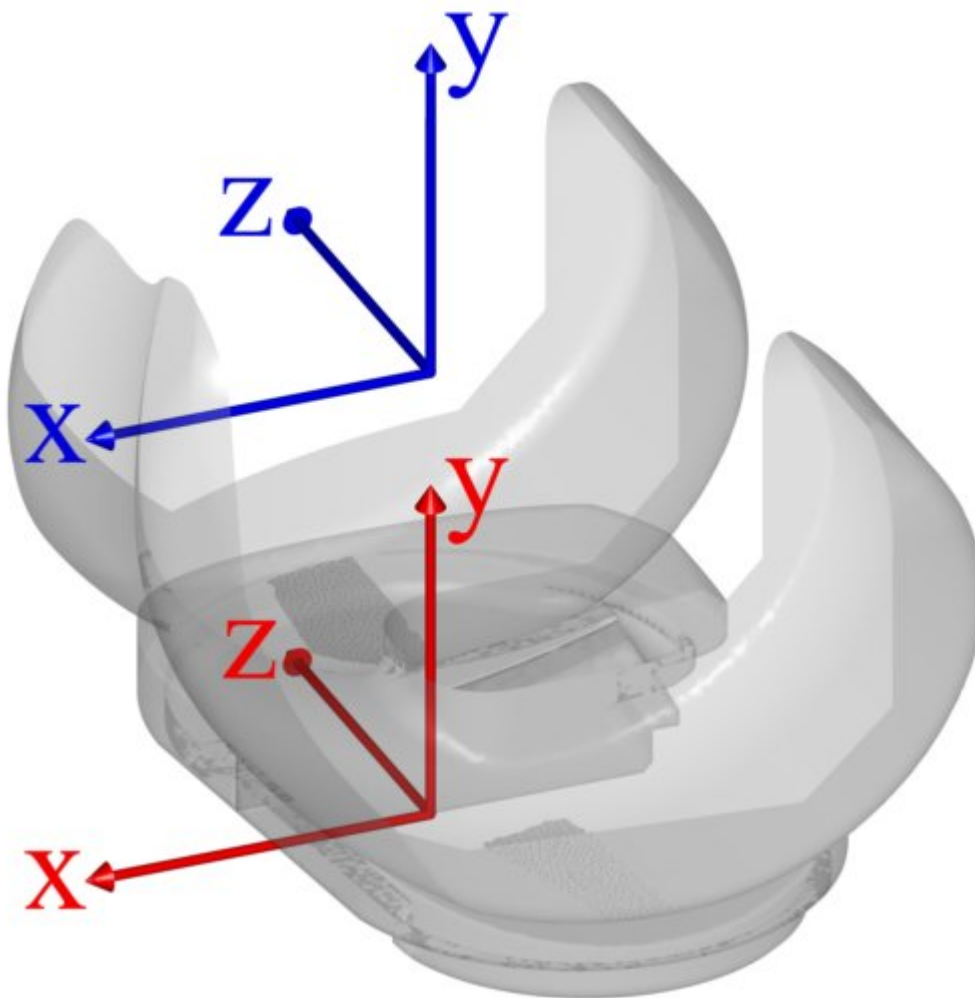
706

708 **Figure 2**

710

Figure 3

712

Figure 4